

# The Gregory-Newton Problem for Kissing Sticky Spheres

Lukas Trombach<sup>1</sup> and Peter Schwerdtfeger<sup>1,2,\*</sup>

<sup>1</sup>Centre for Theoretical Chemistry and Physics, the New Zealand Institute for Advanced Study,  
Massey University Auckland, Private Bag 102904, 0632 Auckland, New Zealand

<sup>2</sup>Centre for Advanced Study (CAS) at the Norwegian Academy of Science and Letters, Drammensveien 78, NO-0271 Oslo, Norway

All possible non-isomorphic arrangements of 12 spheres kissing a central sphere (the Gregory-Newton problem) are obtained for the sticky-hard-sphere (SHS) model, and subsequently projected by geometry optimization onto a set of structures derived from an attractive Lennard-Jones (LJ) type of potential. It is shown that all 737 derived SHS contact graphs corresponding to the 12 outer spheres are (edge-induced) subgraphs of the icosahedral graph. The most widely used LJ(6,12) potential has only one minimum structure corresponding to the ideal icosahedron where the 12 outer spheres do not touch each other. The point of symmetry breaking away from the icosahedral symmetry towards the SHS limit is obtained for general LJ( $a,b$ ) potentials with exponents  $a,b \in \mathbb{R}_+$ . Only if the potential becomes very repulsive in the short-range, determined by the LJ hard-sphere radius  $\sigma$ , symmetry broken solutions are observed.

## I. INTRODUCTION

The arrangement of  $N$  points on the surface of a sphere corresponding to the placement of  $N$  identical non-overlapping spheres around a central sphere is called a spherical packing. To achieve optimal packings for spheres is known as the Tammes problem, originally posed in 1930 to study the distribution of pores on pollen grains [1]: It is to determine the largest diameter and distribution that  $N$  equal non-overlapping spheres may have when packed onto the surface of a sphere of radius 1 (unit sphere). Alternatively, if the centre of each sphere is considered as the vertex of a polyhedron, the graph theoretical problem is to find the polyhedron that maximizes the shortest edge lengths with fixed distance to the central vertex. The Tammes problem has been solved exactly for  $3 \leq N \leq 14$  and  $N = 24$  [2, 3].

Newton and Gregory argued about the maximum possible number  $N_k(d)$  (the *maximum kissing number* or *Newton number*) of three-dimensional unit spheres ( $d = 3$ ) that could be brought into contact with a central sphere [4]. Schütte and van der Waerden provided the first proof in 1953 that  $\max\{N_k(3)\} = 12$  [5]. We call such a cluster of 12 unit spheres kissing a central unit sphere a *Gregory-Newton cluster* (GNC), shown in its most symmetric icosahedral form in Figure 1. Exact Newton numbers for unit spheres in lattice packings are known for dimensions  $d = 1$  to 9 and  $d = 24$ , and for non-lattice packings for  $d = 1 - 3, 8$  and  $24$  [6, 7]. Lower and upper bounds for  $\max\{N_k(d)\}$  are also available [6, 8]. The more general problem of  $N$  spheres of equal radius  $r$  touching a given central sphere of radius 1 in three dimensions has recently been reviewed in detail by Kusner et al. [9]. It is believed that the unit sphere radius  $r = 1$  is the maximal radius where the spheres are arbitrarily permutable with motions remaining on the surface of a central sphere [9].

The Tammes, Thomson or related models employ repulsive forces between points or spheres [10, 11] and, for the three-dimensional problem with 12 kissing spheres, lead to ideal icosahedral symmetry (Figure 1). We may however pose the

question in a slightly different way: What happens if we let the outer kissing spheres of a GNC touch each other to enforce rigidity? We could try to find the global and all local minima for the 12 kissing hard spheres interacting through an attractive instead of a repulsive potential. For example, we can place the central hard sphere in a gravitational field of strength  $F_G = Gm_i m_j r_{ij}^{-2}$  and relax all positions  $r_{ij} \geq (R_i + R_j)$  between the kissing hard spheres  $i$  and  $j$ , in the most general case having sphere radii  $R_i$  and masses  $m_i$ . It is clear that such a procedure leads to a less flexible and more rigid sphere packing. In Euclidian space, this problem is well known to crystallization/sedimentation phenomena modelled by hard spheres in a gravitational field [12, 13].

The most widely used interaction potential in chemical and physical sciences is the so-called Lennard-Jones (LJ) potential [14, 15] (which includes the gravitational potential just mentioned). In reduced units the LJ( $a,b$ ) potential takes the form,

$$V_{a,b}^{\text{LJ}}(r_{ij}) = \frac{ar_{ij}^{-b} - br_{ij}^{-a}}{b-a} \quad (\text{with } r_{ij}, a, b \in \mathbb{R}_+ \text{ and } b > a). \quad (1)$$

It is attractive in the long range and repulsive in the short range. Such a potential maximizes the number of contacts between spheres, and for the famous LJ(6,12) case leads to one and only one minimum for the GNC [16] – the ideal icosahedron (shown in Figure 1) as in the case of the Tammes problem. The icosahedral motif originally proposed by Mackay [17] plays a very important role in cluster physics and chemistry [10, 18–23].

A nice feature of the LJ potential is that for large exponents ( $a,b$ ),  $b > a$ , it approaches the sticky hard-sphere (SHS) limit, originally introduced by Baxter [24, 25],

$$\lim_{a,b \rightarrow \infty} V_{a,b}^{\text{LJ}}(r_{ij}) = V_{\text{SHS}}(r_{ij}) = \begin{cases} \infty & r_{ij} < 1 \\ -1 & \text{for } r_{ij} = 1 \\ 0 & r_{ij} > 1. \end{cases} \quad (2)$$

SHS models have been used intensively in many areas, such as crystallization, flocculation, colloidal suspensions, micelles, protein solutions, or in the exact enumeration of rigid SHS clusters [25–38]. The SHS model has the advantage that an

\* Email: p.a.schwerdtfeger@massey.ac.nz

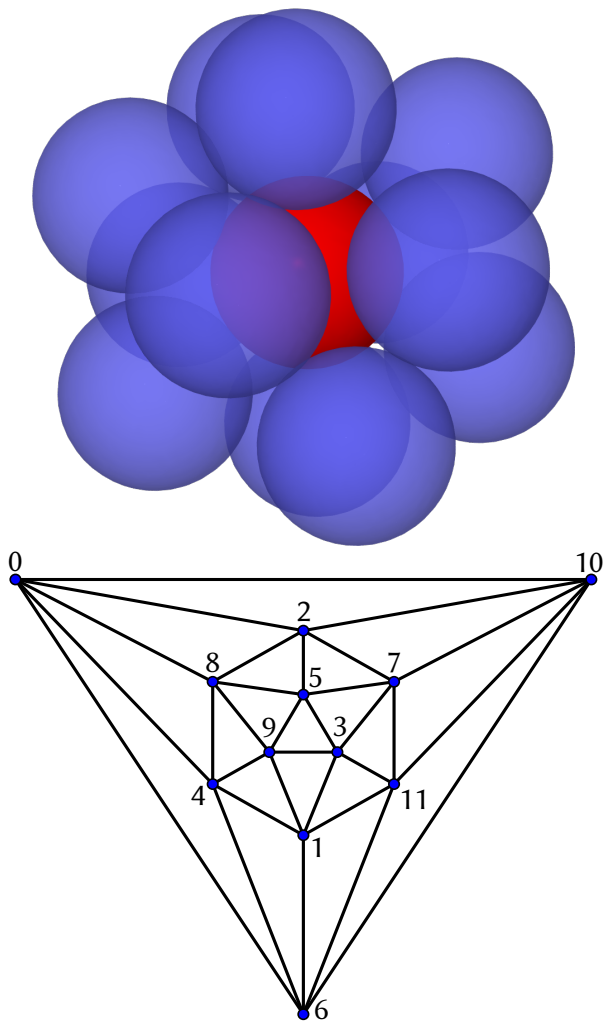


FIG. 1: Top: Symmetric realization of  $N_k(3) = 12$  for unit hard spheres (icosahedral symmetry,  $I_h$ ). The minimum distance between the outer spheres (os) is  $r_{\min}^{\text{os}} = \sin^{-1}\left(\frac{2\pi}{5}\right) = 1.05146222\dots$ , hence they do not touch. Bottom: The corresponding icosahedral graph. Numbering refers to the respective node index used in the Tables S1 and S2 of the Supporting Information.

adjacency matrix  $A$  can be introduced with entries  $A_{ij} = 1$  if spheres  $i$  and  $j$  touch ( $r_{ij} = 1$ ), and 0 otherwise ( $r_{ij} > 1$ ). The number of contacts between spheres then simply becomes  $N_c = \sum_{i < j}^N A_{ij}$ . It also opens the way for a graph-theoretical treatment of cluster structures as we shall see.

A putatively complete set of non-isomorphic rigid sphere packings (SHS clusters) has recently been determined for cluster size  $N \leq 14$  via exact enumeration studies employing geometric rejection and rigidity rules [36, 37, 39]. These include the subset of a rather large number of non-isomorphic rigid GNCs [16]. In addition, the condition  $\lim_{a,b \rightarrow \infty} V_{a,b}^{\text{LJ}}(r) = V_{\text{SHS}}(r)$ ,  $b > a$ , implies that at certain  $a, b$  values symmetry broken solutions away from the ideal icosahedral structure must appear. Where exactly this happens, and when the icosahedral structure does not survive anymore, is not known. In

order to close this gap, we decided to analyse the rigid GNCs and corresponding symmetry breaking effects in detail. This is much in the spirit of Wales, who already pointed out that the global characteristics of the energy landscape of a cluster can be quite sensitive to the nature of the interatomic potential applied [40].

## II. COMPUTATIONAL METHODS

Coordinates for GNC structures have been obtained by searching for adjacency matrices of the results for  $N = 13$  from Ref. [36] with one row or column containing twelve "1" entries. Sub-graph isomorphism was verified using the *VF2* algorithm [41] as implemented in the *boost graph library* [42]. Structural optimisations with LJ potentials have been carried out using the multidimensional function minimiser from the C++ library *dlib* [43] and an energy convergence criterion of  $10^{-15}$ . Results from the optimisation procedure were analysed based on the Euclidean distance matrix, which is unique for non-isomorphic structures apart from permutation, translation, rotation and inversion. For this we sorted the distances lexicographically.

## III. RESULTS AND DISCUSSION

### A. Rigid Gregory-Newton Clusters and Corresponding Graphs

The recent results by Holmes-Cerfon [36] contain a putatively complete set of rigid (and few semi-rigid) SHS clusters of size  $N = 13$  and  $N = 14$  (for details on the near completeness of the set of rigid clusters obtained see the discussion in Ref.[36]). The rigid GNCs can easily be identified as a subset of the set of all non-isomorphic rigid SHS clusters, i.e.  $\{S_{\text{GN}}\} \subset \{S_{\text{SHS}}\}$ ; these have adjacency matrices  $A$  with exactly one column and row containing twelve "1" entries due to 12 spheres kissing the central sphere (as these cluster lie in the region of high contact numbers with  $N_c \geq 3N - 6$ , we expect that the set is most likely complete). A surprisingly large number of 737 non-isomorphic  $N = 13$  GNCs out of 98,540 rigid SHS clusters can be found [16]. There are four different possible contact numbers  $N_c$  with  $\{724, 10, 1, 2\}$  rigid GNCs corresponding to  $N_c = \{33, 34, 35, 36\}$ , therefore, non of those clusters are hypostatic.

For further analysis and without loss of generality we delete the central sphere and analyse the remaining non-isomorphic shell of spheres (note that rigidity requires the presence of the central sphere), also called contact graphs according to Schütte, van der Waerden and Habicht [44]. This has the advantage that these shells are related to planar connected graphs. In the following we call the corresponding connected, planar graph of such a shell of spheres with the central sphere missing a *GN graph*. The question arises if all 737 non-isomorphic GN graphs are subgraphs to the icosahedral graph, as shown in Figure 1. This would make sense as it is impossible to increase the degree of any vertex beyond 5 in the

GN graph. Note that the icosahedral cluster is completely unjammed and its space of (infinitesimal) deformations has dimension 24 (for details see Ref.[9]).

Employing the VF2 algorithm [41] as implemented in the *boost graph library* [42] we find all 737 non-isomorphic GN graphs  $G_{GN}(V, E')$  (vertex count  $|V| = 12$ , edge count  $|E'| < 30$ ) to be (edge-induced) subgraphs of the icosahedral graph  $G_{ico}(V, E)$  ( $|V| = 12$ ,  $|E| = 30$ ), which implies that their vertices can all be mapped to vertices of the icosahedral graph with certain edges deleted such that the subgraph remains connected ( $V_{GN} = V_{ico}$  and  $E_{GN} \subset E_{ico}$ ). An extensive list of all subgraphs is included in the Supporting Information (Tables S1 and S2). Note, not all GN graphs are 3-connected and therefore are not strictly polyhedral according to Steinitz's theorem [45]. These are the graphs which have vertices of degree 2, i.e.  $|V_2| > 0$ , and there are 304 of them, Table S1. As the many non-isomorphic graphs listed in the SI are obtained from a certain combination of edge deletions under the constraint of maintaining rigidity, it is not surprising at all that the number of non-isomorphic GN graphs is so large.

The results show, that at least six and up to a maximum of nine edges have to be removed from the icosahedral graph to create a GN graph. Removing six edges from the icosahedral graph results in 24 edges, or  $N_c = 36$  if we include the central sphere. For  $N = 13$  this is exactly equal to  $3N - 3$  which is the maximum contact number observed for this cluster size [36, 39]. Consequently, removing nine edges gives  $N_c = 33 = 3N - 6$ , meaning that rigid GNCs cannot be hypostatic (i.e.  $N_c < 3N - 6$ ). Interestingly, there are only two graphs with maximum edge count of  $|E| = 24$ , which are exactly the fragments of the face-centered cubic (fcc, ABCABC... layers) and hexagonal closed packed (hcp, ABAB... layers) bulk structures, respectively. These are the result from removing 6 edges in such a way, that exactly one edge is removed from every vertex in the icosahedral graph (thus the degree of every vertex is 4), see Figure 2. Removing edges in this way implies that the resulting two graphs consist of triangles and rectangles only. The difference between the fcc and hcp clusters is in the way their square faces are connected; in the fcc case the square faces only connect via edges (cuboctahedron), while in hcp case the square faces come in pairs sharing one edge (triangular orthobicupola or Johnson solid  $J_{27}$ ) [9].

The construction of hcp and fcc structures by a continuous deformation of an icosahedron has been described in detail by Kusner et al. [9] and goes back to Conway and Sloane in 1988 [6]. We note that hcp and fcc can both be obtained from a rearrangement of the spheres in an icosahedron by forming a (zig-zag) cycle (closed path) through six vertices, and arranging those spheres on the path such that they are in-plane with the central sphere, which becomes part of the hexagonal plane as in the bulk fcc and hcp packing (Figure 3). Additionally, the plane has to be rotated by  $\pi/6$  to create the fcc structure. The hcp structure can be constructed by also rotating either the top or the bottom plane by the same amount in either direction parallel to the hexagonal plane. Kusner noted that a smooth deformation from the icosahedral configuration to hcp requires 9 moving spheres [9]. This interesting transi-

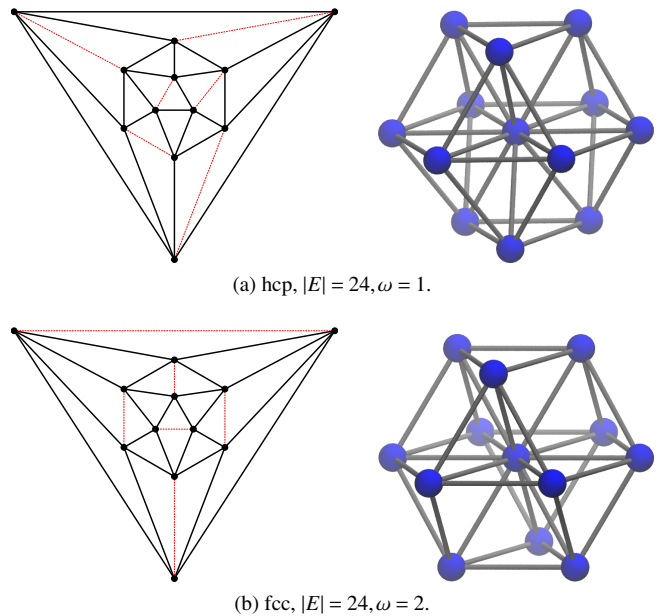


FIG. 2: GN hcp (triangular orthobicupola) and fcc (cuboctahedron) graphs (central sphere removed) as subgraphs of the icosahedral graph and corresponding rigid GNCs. Red lines indicate the edges that were removed to create the GN graph. The ordinal numbers  $\omega$  refer to Table S2 in the SI.

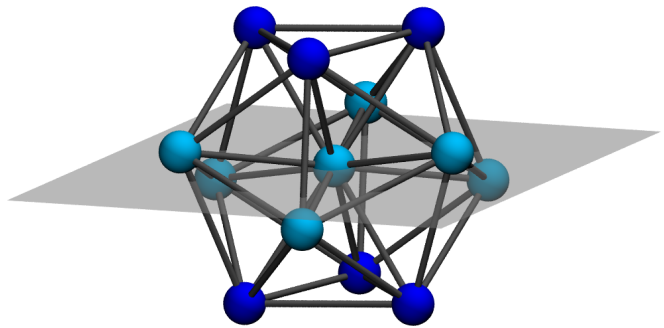


FIG. 3: Illustration of one zig-zag path (light blue spheres) that needs to be deformed such that it aligns with the triangular plane (shown in grey) of the fcc crystal.

tion path may be the key for the icosahedral to closed-packed rearrangements in larger clusters, which has previously been described in terms of catastrophe theory as a cusp catastrophe [40].

Even though the rearrangement from the icosahedral to either the fcc or hcp cluster structure can easily be realized for the GNC, there should be clusters where the icosahedral motif is still clearly visible, i.e. only small rearrangements of the spheres are necessary to break icosahedral symmetry and form a rigid cluster. These are, for example, the ones with maximum count of triangles, i.e. according to Table S1 (SI) the GN graphs with  $|F_3| = 10$  with edge counts of  $|E| = 22$  or 21. Two of these are shown with their corresponding graphs in Figure 4.

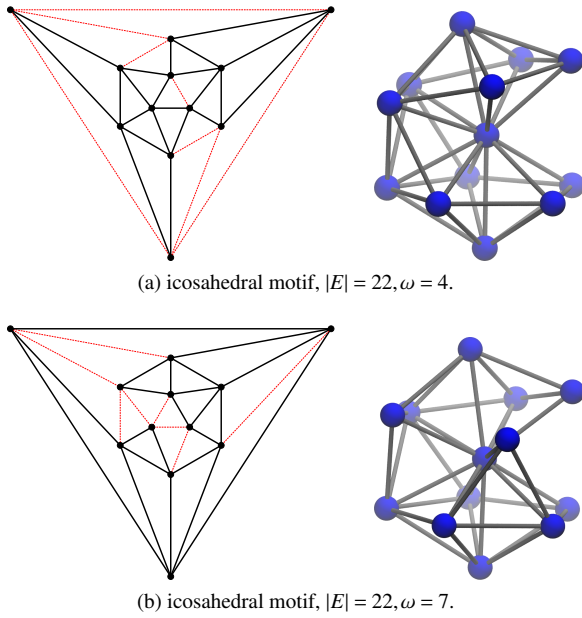


FIG. 4: Representative GN graphs (central sphere removed) with  $|F_3| = 10$  as subgraphs of the icosahedral graph and corresponding rigid GNCs. The icosahedral motif in the 3D embedding is clearly visible. Red lines indicate the edges that were removed to create the GN graph. The ordinal numbers  $\omega$  refer to Table S2 in the Supporting Information.

Figure 5 shows the graph with the next highest edge count after the fcc and hcp packings. The motif of a distorted elongated pentagonal bipyramid (Johnson solid  $J_{16}$ ) is clearly visible. Note that the Johnson solid can be obtained by deleting five edges in the icosahedral graph and rotating the two opposite pentagonal pyramids by  $2\pi/5$ . One of the resulting square faces has to be stretched to obey the SHS conditions, which is achieved by removing two additional edges. In the graph this implies that a hexagonal face is formed. Note that this GNC is also the cluster with the largest distance  $r_{\max}^{\text{RE}} = 1.47823719$  that corresponds to a removed edge (RE) in the GN graph. Capping this cluster with one more sphere over the distorted square face with  $r_{\max}^{\text{RE}}$  leads to the structure with the shortest distance to the central sphere a sphere in the second coordination shell can have ( $r^{\text{COS}} = 1.347150628$ ) out of all 14,529 GN clusters with  $N = 14$  [16].

If more edges are removed from the icosahedral graph we see the appearance of larger  $n$ -gonal faces with the largest face being a 12-gon.

### B. Symmetry-Broken Lennard-Jones Gregory-Newton Clusters

All 737 non-isomorphic rigid GNCs optimise to the ideal icosahedral symmetry if a LJ(6,12) potential is applied [16] (however, for larger sized icosahedral structures many more minima appear, see Refs. [46–49]). As mentioned in the introduction, for equally sized hard spheres a cluster with icosahedral symmetry leaves gaps between the spheres on the outer shell, i.e. they do not touch, and is therefore not considered rigid under SHS conditions. Hence, at certain  $(a, b)$  combinations a phase transition must occur in the LJ( $a, b$ ) energy landscape where local minima appear, which do not have icosahedral symmetry anymore. In order to determine those  $(a, b)$  combinations, we optimised all 3D cluster geometries with varying exponents ( $6 \leq a \leq 34$  and  $7 \leq b \leq 35$ ) with  $(b > a)$  and analysed the number of resulting minimum structures. The results are shown schematically in Figure 6.

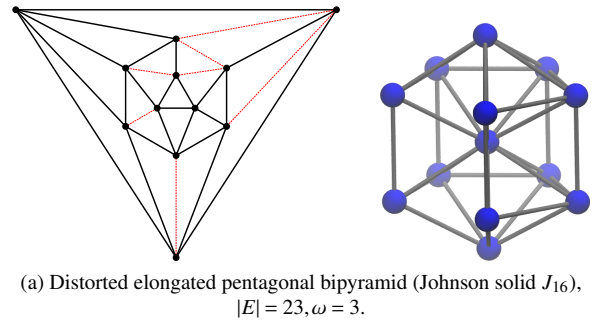


FIG. 5: GN graph (central sphere removed) as subgraphs of the icosahedral graph and corresponding GN Johnson-like solid (with edges removed). Red lines indicate the edges that were removed from the icosahedral graph to create the GN graph. The ordinal number  $\omega$  refers to Table S2 in the Supporting Information.

hedral symmetry leaves gaps between the spheres on the outer shell, i.e. they do not touch, and is therefore not considered rigid under SHS conditions. Hence, at certain  $(a, b)$  combinations a phase transition must occur in the LJ( $a, b$ ) energy landscape where local minima appear, which do not have icosahedral symmetry anymore. In order to determine those  $(a, b)$  combinations, we optimised all 3D cluster geometries with varying exponents ( $6 \leq a \leq 34$  and  $7 \leq b \leq 35$ ) with  $(b > a)$  and analysed the number of resulting minimum structures. The results are shown schematically in Figure 6.

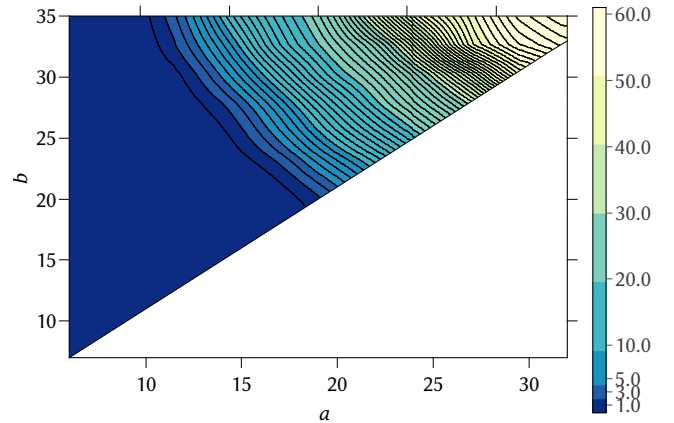


FIG. 6: Number of unique structures resulting from an optimisation with a LJ( $a, b$ ) potential. The lowest contour line shows the point where more than one structure results from the optimisation and the distance between contour lines is 1.

Figure 7 contains additional information showing three major phase transitions in the topology of the energy landscape going from low to high  $(a, b)$  exponents. In the blue shaded area (1), the Mackay icosahedron is the sole minimum in the potential energy landscape. The first transition occurs when this symmetry can be broken, and other local minima are supported by the LJ( $a, b$ ) potential besides the icosahedron. This is indicated in Figure 7 by the smallest, orange region (2),

which still contains the perfect icosahedron as the global minimum. At slightly higher exponents, other structures become energetically more favourable and replace the icosahedron as the global minimum, region (3). However, the icosahedron remains as a local minimum in the potential energy surface. The last transition occurs when the LJ potential becomes SHS-like, and the icosahedral cluster completely disappears from the potential energy surface, region (4). The three transition lines are generally smooth.

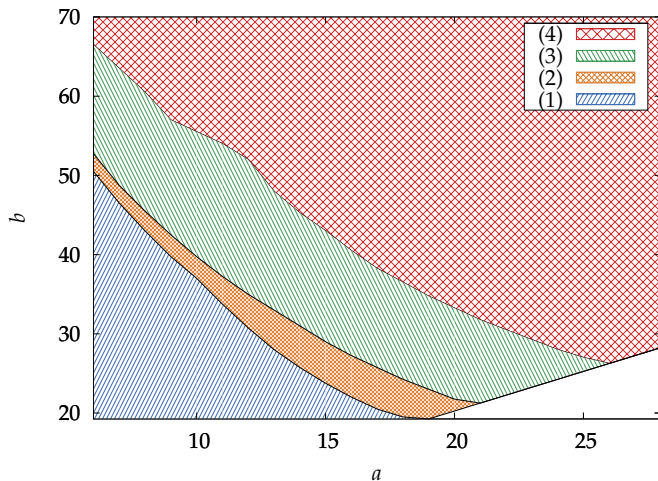


FIG. 7: Different types of energy landscapes arising from combinations of the LJ  $(a, b)$  exponents. (1) One single (icosahedral) minimum, (2) more than one minimum with the icosahedron as the global minimum, (3) more than one minimum with the icosahedron becoming a local (and not global) minimum, (4) the icosahedral motif disappears completely. The unshaded small area in the bottom right corner corresponds to  $a > b$ , which is excluded. The resolution for  $a$  is 1.0 and for  $b$  0.25.

Figure 8 shows representative LJ potentials for combinations of the  $(a, b)$  exponents (with low and high  $a$  values) on the phase transition lines drawn in figure 7. At these phase transition lines, the corresponding LJ potentials show narrow and steep repulsive potentials compared to the LJ(6, 12) potential, which all look very similar in the short range ( $r < 1$ ). However, they differ substantially in the long range ( $r > 1$ ).

The  $(a, b)$  parameters can be related to the so-called LJ hard-sphere radius  $\sigma$  (given by the intersection with the abscissa) through equation (1),

$$\sigma = \left(\frac{b}{a}\right)^{\frac{1}{a-b}}. \quad (3)$$

and we only have to consider the  $(a, \sigma)$  combinations shown in Figure 9 along the phase transition lines.

The variation in  $\sigma$  along the phase transitions lines for  $(2) \rightarrow (3)$  and  $(3) \rightarrow (4)$  are rather small. However, all three transitions clearly show different ranges for  $\sigma$  and thus can be characterized by the LJ hard-sphere radius. These are also much larger compared to the LJ(6, 12) hard-sphere radius of  $\sigma = 0.891$ , and close to the ideal hard sphere radius of 1 within

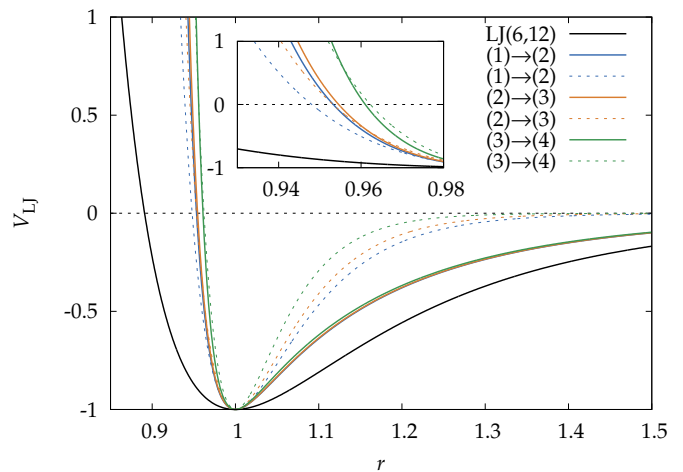


FIG. 8: Comparison of different shapes of LJ potentials at the phase transition lines shown in fig. 7 with the traditional LJ(6, 12) potential (black solid line). Dashed lines refer to potentials with low  $a$  values (left side of fig. 7), while solid lines refer to potentials with high  $a$  values (right side of fig. 7).

the SHS model. This demonstrates that the shape of the LJ potential in the repulsive region has a significant influence on the position of the transition lines, and therefore on the topology of the energy landscape. In contrast, these transitions seem to be far less affected by the shape of the potential in the attractive region. Only for the transition  $(1) \rightarrow (2)$  we see a larger variation in  $\sigma$ .

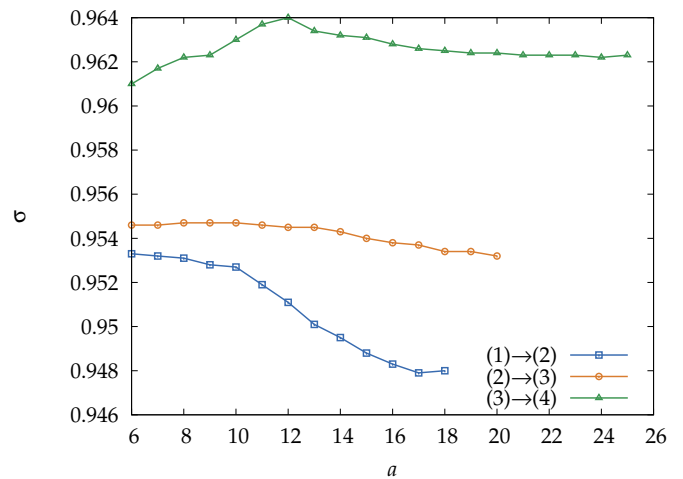


FIG. 9: Hard-sphere radii  $\sigma$  in reduced units for the LJ  $(a, b)$  potentials on the transition lines shown in fig. 7.

Of course, symmetry breaking (such as Jahn-Teller distortions) in icosahedral clusters is well known in cluster chemistry and physics [50], which, however, requires the introduction of many-body forces beyond the usual two-body interaction, or a correct quantum theoretical treatment containing all many-body forces.

#### IV. CONCLUSIONS

We have analysed rigid GNCs by graph theoretical means. All 737 non-isomorphic GN graphs are subgraphs of the icosahedral graph obtained by deleting a minimum of 6 and a maximum of 9 edges. There are only two structures with maximum edge count of 24 corresponding to the sphere packing of the fcc and hcp structures, which can be obtained from the icosahedral structure by a smooth rearrangement moving the six spheres along a closed zig-zag path into the (hexagonal) plane. The common LJ(6,12) potential has only one minimum structure corresponding to the ideal icosahedron where the 12 outer spheres do not touch each other. Symmetry breaking requires a very repulsive short-range LJ potential. We also determined the  $(a,b)$ -line in the LJ( $a,b$ ) potential where the icosahedron completely disappears. While our results depend on the functional form chosen (the Lennard-Jones potential), we expect similar results for other well known potentials such as the Morse potential.

The sphere kissing problem in higher dimensions is a

well known problem [6] (in two dimensions there is only 1 non-isomorphic GNC). How many non-isomorphic rigid GNCs there are in greater than three dimensions is currently unknown. Moreover, the rigid kissing sphere problem can be extended to other (convex or not) topologies instead of a central sphere, e.g. kissing spheres on an ellipsoid. There are many open questions in this field.

#### V. ACKNOWLEDGEMENTS

We acknowledge financial support, including covering the costs to publish in open access, by the Marsden Fund of the Royal Society of New Zealand and the Centre for Advanced Study at the Norwegian Academy of Science and Letters (Molecules in Extreme Environments Research Program). We thank Profs. David J. Wales (Cambridge) and Robert S. Hoy (Tampa) for valuable comments.

- 
- [1] P. M. L. Tammes, *Recueil des travaux botaniques néerlandais* **27**, 1 (1930).
- [2] R. M. Robinson, *Math. Ann.* **144**, 17 (1961).
- [3] O. R. Musin and A. S. Tarasov, *Exp. Math.* **24**, 460 (2015), <https://doi.org/10.1080/10586458.2015.1022842>.
- [4] F. Pfender and G. M. Ziegler, *Notices - Am. Math. Soc.* **51**, 873 (2004).
- [5] K. Schütte and B. L. van der Waerden, *Math. Ann.* **125**, 325 (1952).
- [6] J. H. Conway and N. J. A. Sloane, *Sphere Packings, Lattices and Groups*, 3rd ed., Grundlehren der mathematischen Wissenschaften No. 290 (Springer Science & Business Media, 2013).
- [7] O. R. Musin, arXiv preprint arXiv:1712.04099 (2017).
- [8] H. Mittelmann and F. Vallentin, *Exp. Math.* **19**, 175 (2010).
- [9] R. Kusner, W. Kusner, J. C. Lagarias, and S. Shlosman, arXiv:1611.10297 [math.MG] (2016), arXiv:1611.10297 [cond-mat].
- [10] D. J. Wales and S. Ulker, *Phys. Rev. B* **74**, 212101 (2006).
- [11] D. J. Wales, H. McKay, and E. L. Altschuler, *Phys. Rev. B* **79**, 224115 (2009).
- [12] Y. Levin, *Physica A: Statistical Mechanics and its Applications* **287**, 100 (2000).
- [13] P. N. Pusey, E. Zaccarelli, C. Valeriani, E. Sanz, W. C. K. Poon, and M. E. Cates, *Philosophical Transactions of the Royal Society of London A: Mathematical, Physical and Engineering Sciences* **367**, 4993 (2009), <http://rsta.royalsocietypublishing.org/content/367/1909/4993.full.pdf>
- [14] J. E. Jones, *Proc. Royal Soc. London A: Math., Phys. Eng. Sci.* **106**, 463 (1924).
- [15] J. E. Lennard-Jones, *Proc. Phys. Soc.* **43**, 461 (1931).
- [16] L. Trombach, R. S. Hoy, D. J. Wales, and P. Schwerdtfeger, *Phys. Rev. E* **97**, 043309 (2018).
- [17] A. L. Mackay, *Acta Cryst.* **15**, 916 (1962).
- [18] M. R. Hoare and P. Pal, *Advances in Physics* **24**, 645 (1975).
- [19] T. D. Klots, B. J. Winter, E. K. Parks, and S. J. Riley, *J. Chem. Phys.* **92**, 2110 (1990).
- [20] J. Uppenbrink and D. J. Wales, *J. Chem. Soc. - Faraday Trans.* **87**, 215 (1991).
- [21] B. W. van de Waal, *J. Chem. Phys.* **98**, 4909 (1993).
- [22] D. J. Wales, L. J. Munro, and J. P. K. Doye, *J. Chem. Soc., Dalton Trans.*, 611 (1996).
- [23] D. J. Wales and L. J. Munro, *J. Chem. Phys.* **100**, 2053 (1996).
- [24] R. J. Baxter, *J. Chem. Phys.* **49**, 2770 (1968).
- [25] D. Gazzillo and A. Giacometti, *J. Chem. Phys.* **120**, 4742 (2004), <https://doi.org/10.1063/1.1645781>.
- [26] G. Stell, *J. Stat. Phys.* **63**, 1203 (1991).
- [27] A. Jamnik, *J. Chem. Phys.* **105**, 10511 (1996), <https://doi.org/10.1063/1.472940>.
- [28] A. Santos, S. B. Yuste, and M. L. de Haro, *J. Chem. Phys.* **109**, 6814 (1998), <https://doi.org/10.1063/1.477328>.
- [29] R. S. Hoy and C. S. O'Hern, *Phys. Rev. Lett.* **105**, 068001 (2010).
- [30] N. Arkus, V. N. Manoharan, and M. P. Brenner, *Phys. Rev. Lett.* **103**, 118303 (2009).
- [31] G. Meng, N. Arkus, M. P. Brenner, and V. N. Manoharan, *Science* **327**, 560 (2010).
- [32] N. Arkus, V. Manoharan, and M. Brenner, *SIAM J. Discrete Math.* **25**, 1860 (2011).
- [33] R. S. Hoy, J. Harwayne-Gidansky, and C. S. O'Hern, *Phys. Rev. E* **85**, 051403 (2012).
- [34] B. Hayes, *Am. Scientist* **100**, 442 (2012).
- [35] M. Holmes-Cerfon, S. J. Gortler, and M. P. Brenner, *Proc. Natl. Acad. Sci. U.S.A.* **110**, E5 (2013), 23248296.
- [36] M. Holmes-Cerfon, *SIAM Review* **58**, 229 (2016).
- [37] M. Holmes-Cerfon, *Ann. Rev. Cond. Matter Phys.* **8**, 77 (2017).
- [38] Y. Kallus and M. Holmes-Cerfon, *Physical Review E* **95**, 022130 (2017).
- [39] R. S. Hoy, *Physical Review E* **91**, 012303 (2015).
- [40] D. J. Wales, *Science* **293**, 2067 (2001).
- [41] L. P. Cordella, P. Foggia, C. Sansone, and M. Vento, *IEEE Transactions on Pattern Analysis and Machine Intelligence* **26**, 1367 (2004).

- [42] J. Siek, L.-Q. Lee, and A. Lumsdaine, *The Boost Graph Library: User Guide and Reference Manual*, !! (Addison-Wesley Longman Publishing Co., Inc., Boston, MA, USA, 2002).
- [43] D. E. King, *Journal of Machine Learning Research* **10**, 1755 (2009).
- [44] K. Schütte and B. L. van der Waerden, *Math. Ann.* **123**, 96 (1951).
- [45] E. Steinitz, *Enzyklopädie der mathematischen Wissenschaften*, Band 3 (Geometries) **3**, 1 (1922).
- [46] J. P. K. Doye, D. J. Wales, and R. S. Berry, *J. Chem. Phys.* **103**, 4234 (1995), <https://doi.org/10.1063/1.470729>.
- [47] D. J. Wales and J. P. Doye, in *Large Clusters of Atoms and Molecules* (Springer, 1996) pp. 241–279.
- [48] J. P. K. Doye and D. J. Wales, *J. Phys. B: At. Mol. Opt. Phys.* **29**, 4859 (1996).
- [49] J. P. K. Doye and D. J. Wales, *J. Chem. Soc., Faraday Trans.* **93**, 4233 (1997).
- [50] W. A. de Heer, *Rev. Mod. Phys.* **65**, 611 (1993).